

Article

# Increasing the Lateral Resolution of 3D-GPR Datasets through 2D-FFT Interpolation. Application to the Case Study of Roman Villa of Horta Da Torre (Fronteira, Portugal)

Rui Jorge Oliveira <sup>1,2,3,\*</sup>, Bento Caldeira <sup>1,2,3</sup>, Teresa Teixidó <sup>4</sup>, José Fernando Borges <sup>1,2,3</sup> and André Carneiro <sup>5,6</sup>

<sup>1</sup> Instituto de Ciências da Terra, ICT, Universidade de Évora, Apartado 94, 7002-554 Évora, Portugal; bafcc@uevora.pt (B.C.); jborges@uevora.pt (J.F.B.)

<sup>2</sup> Departamento de Física, Escola de Ciências e Tecnologia, Universidade de Évora, Apartado 94, 7002-554 Évora, Portugal

<sup>3</sup> Earth Remote Sensing Laboratory, EaRSLab, Universidade de Évora, Apartado 94, 7002-554 Évora, Portugal

<sup>4</sup> Instituto Andaluz de Geofísica, Campus Universitario de Cartuja, Universidad de Granada, 18071 Granada, España; tteixido@ugr.es (T.T.)

<sup>5</sup> Departamento de História e Arqueologia, Escola de Ciências Sociais, Universidade de Évora, Apartado 94, 7002-554 Évora, Portugal; ampc@uevora.pt (A.C.)

<sup>6</sup> Centro de História da Arte e Investigação Artística, Universidade de Évora, Apartado 94, 7002-554 Évora, Portugal

\* Correspondence: ruio@uevora.pt (R.J.O.)

**Abstract:** INT-FFT algorithm presented in this work uses an interpolation methodology to densify 3D-GPR datasets to sharpen images obtained in GPR surveys obtained in an archaeological context. It allows the reconstruction of missing data from the combined use of mathematical transforms (e.g., the Fourier and Curvelet transform) and predictive filters. This technique makes it possible to calculate the missing signal simply by meeting two requirements: the data in the frequency domain must be limited in a range of values and must be able to be represented by a distribution of Fourier coefficients (verified conditions). The INT-FFT algorithm uses an open-access routine (*Suinterp*, Seismic Unix) to interpolate the GPR profiles based on seismic trace interpolation. This process uses automatic event identification routines by calculating spatial derivatives to identify discontinuities in space by detecting very subtle changes in the signal, thus allowing for more efficient interpolation without artifacts or signal deterioration. We successfully tested the approach using GPR datasets from the Roman Villa of Horta da Torre (Fronteira, Portugal). The results show an increase in the geometric sharpness of the GPR reflectors and have not produced any numerical artifacts. The tests performed to apply the methodology to GPR-3D data allowed for assessing the interpolation efficiency, the level of recovery of missing data, and the level of information lost when one chooses to increase the distance between profiles in the acquisition stage of the data.

**Keywords:** applied geophysics; digital signal processing; enhancement of sharpness of 3D-GPR datasets; 2D Fourier interpolation; GPR data densification

## 1. Introduction

### 1.1. Ground-Penetrating Radar in Archaeologic Exploration

Geophysical methods to prospect the subsurface in an archaeological environment are essential for remote sensing study non-invasive and non-destructive. These features can increase the knowledge about an archaeological site and play an essential role in the site planning, which can turn the protection endeavors of the heritage more effective.

Among the various methods available, ground-penetrating radar (GPR) is one of the most common electromagnetic methods used in Geophysics applied to Archaeology. It has become more popular since 1970 [1] due to its advantages of quick data acquisition and high resolution. This method allows the determination of the spatial distribution of buried structures in the ground, such as walls, ditches, floors, cavities, and even water

levels. We achieve the information by propagating an electromagnetic wave (EMW) in the ground with a known frequency. The typical frequency values for archaeological prospection vary between 200 MHz and 1.6 GHz [2]. Among several requirements to apply GPR to obtain the desired data, there is a need to control some aspects of the acquisition, the field procedure, and the parameterization of the equipment. In acquisitions in 3D mode through parallel profiles, an adequate parameterization includes pin a set of requirements as the orientation of the profiles, the number of samples per trace, trace separation, temporal range, and gain adjustment. The number of profiles to acquire is also one of the characteristics to choose which consequences acquisition time and data quality. The operator must choose this parameter to compromise the survey execution time and the quality of the acquired data. A longer distance between profiles reduces the acquisition time but can prevent the detection of reflectors corresponding to buried structures. The task of defining these parameters requires careful consideration.

### 1.2. Archaeological site: Roman Villa of Horta da Torre (Fronteira, Portugal)

The Roman Villa of Horta da Torre is located at Fronteira municipality (Alentejo, Portugal) (Figure 1a). This archaeological site belongs to the former Roman province of Lusitania. There are other *villae* examples in the surroundings with similar monumental *pars urbanae* surrounded by buildings for agricultural operations [3].

Horta da Torre is an excellent example of an opulent classical *villa* (Figure 1b-c), with good construction, high monumentality, and quality of structural elements. The building is on a gentle slope, facing south and west, with excellent visibility, plenty of water resources, great pedological variety, and its *diverticulum*. It is approximately 500 meters from the XIV route, a principal Antonine route between Olisipo (Lisboa, Portugal) and Augusta Emerita (Mérida, Spain).

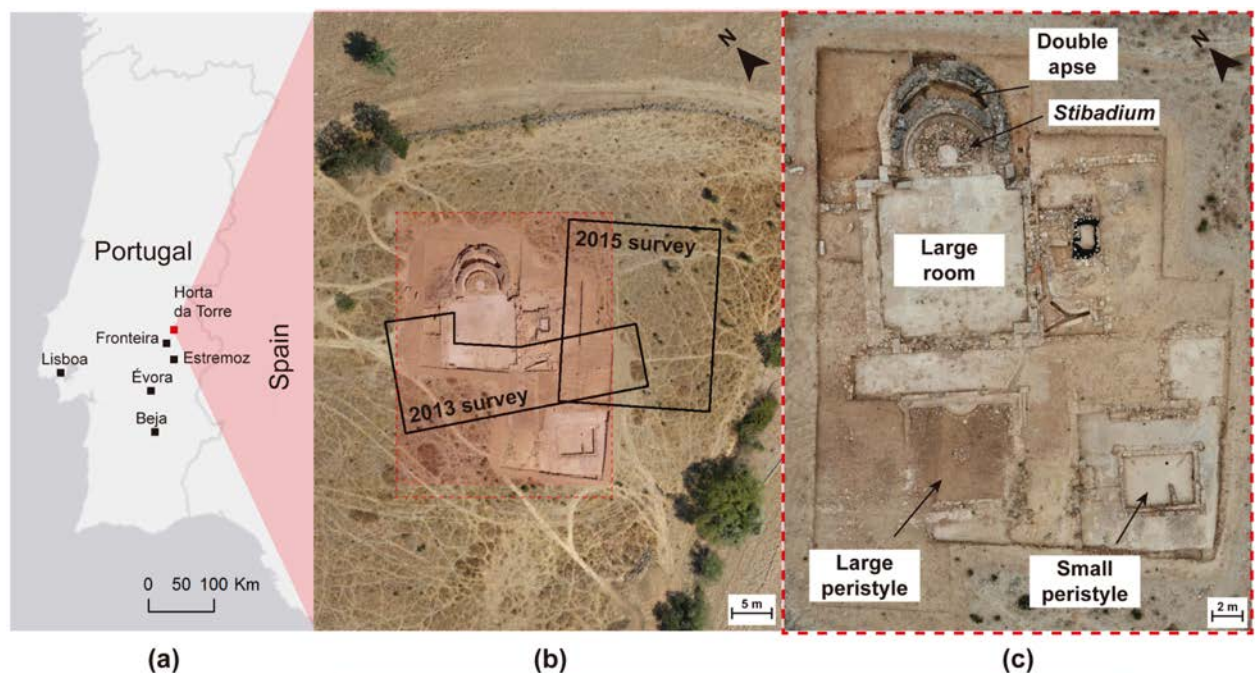


**Figure 1.** (a) Geographical location of Horta da Torre. (b) General overview of the archaeological site and representation of the GPR surveys performed in 2013 and 2015. (c) Orthophoto of Horta da Torre remains taken in 2019, showing the status of the excavation.

We only know of three structural cores as of 2012: the Bath, a 15x25 m tank with an *opus signinum* covering, which has two partially preserved walls and a third tomb; the Tower, an excellent apse structure that was interpreted as a part of a thermal building or to the *pars urbanae* of the villa; and the Mosque, a mosaic-covered apse, far from the central nucleus. About 30 m south of Bath, we identified extensive floors of *opus signinum*.

After 2012, the excavations revealed the existence of structures such as walls and pavements (Figure 2). Close to the apse structure, a *stibadium* was discovered, located at the back of a richly decorated room, and covered by large slabs of white marble. Only traces discovered were at the bottom. These would be covered with *opus tessellatum* on the walls or ceiling according to many traces of fragmented mosaics found in an inverted position in the layer of sediment that covers the space of the room. The excavation reveals that the *stibadium* crowned a room with running water throughout the room, released by a hatch hidden in the apse behind the *stibadium*. This one had a robust and high-quality *opus signinum* floor with a half-round around the baseboard connected to the marble slabs. Next to this room, there is a large *perystilium*. At the base of the columns is a wall with a water pipe inside. There is also a smaller *perystilium*, suggesting that it may have a more personal character than the other structures.

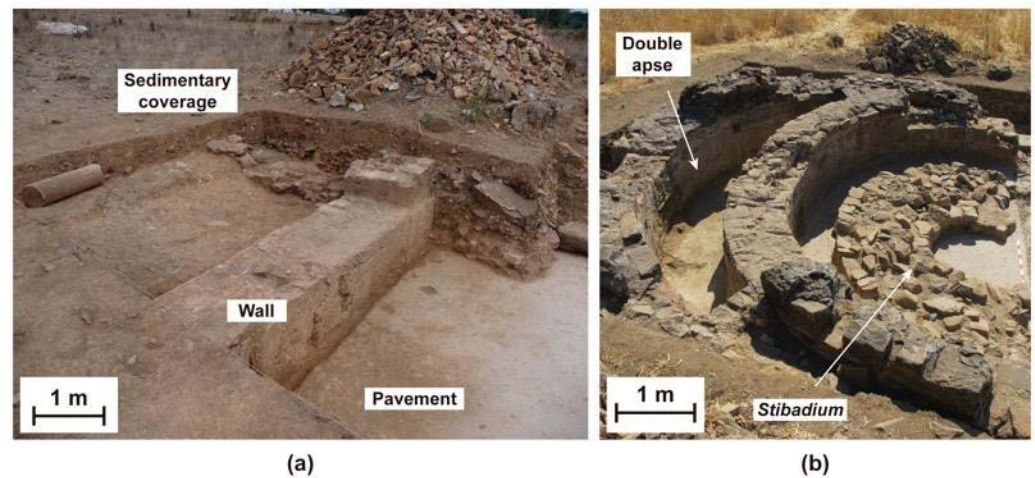


**Figure 2.** (a) Wall and pavement excavated after the 2013 GPR survey. (b) Double apse and *stibadium* remain [3]. All the unearthed traces show great grandeur and robustness.

### 1.3. GPR Surveys Performed in the Site

Around the double apse structure, two GPR survey areas were defined (Figure 1b). The first survey, carried out in 2013, was performed with a profile spacing of 0.25 m. Because a portion of this space lies on an excavated section of the site, it has an uneven shape. The profiles have a maximum length of 31.0 m, acquired in a width of 14.5 m. The second survey, carried out in 2015, was performed with a profile spacing of 0.50 m. Obstacles such as dense bushes and stones contributed to the increase in the distance between the profiles compared to the previous study. As a result, this area has a regular shape, with dimensions of 19.0 m and 22.9 m. Table 1 lists the configuration parameters for both acquisitions.

The GPR datasets had a standard processing flow that allowed the best interpretation of buried structures in the site (detailed in Table 2). It includes correction of the surface position, infinite impulse response (IRR) filters, constant gain adjustment, migration, deconvolution, finite impulse response (FIR) filters, linear gain adjustment, and Hilbert transform. GSSI RADAN 6.5 is the software to implement this processing sequence. The last operation consisted of generating 3D volume, often referred to as the 2.5D model, from where extracted depth-slices at several depths with the same thickness. Finally, from all depth-slices, cover surfaces [4] of both datasets were calculated and overlapped to an aerial orthophoto (Figure 3). The cover surface is a layer that relates the reflection amplitude of the depth-slices with their depth, giving a depth perspective of the amplitude distribution.

**Table 1.** Acquisition parameters of GPR surveys.

Acquisition parameters	2013 survey	2015 survey
Number of profiles	59	39
Distance between profiles (m)	0.25	0.50
Antenna frequency (MHz)	400	400
Scans per meter	50	40
Samples per trace	1024	1024
Temporal depth (ns)	100	50
IIR band-pass filter (MHz)	100 - 800	100 - 800

**Table 2.** Processing parameters of GPR datasets, performed in the GSSI RADAN software.

Processing operation	2013 survey	2015 survey
Correction of the surface position		5.37 ns
IIR filters	11 traces	13 traces
Gain adjustment	Constant in time window	
Kirchhoff migration	Width 11; velocity 0.04 m/ns	
Predictive deconvolution	N=17; Predictive lag=3	
FIR filters	295-580 MHz	
Gain adjustment	Linear, 7 points	
Hilbert transform	Magnitude	

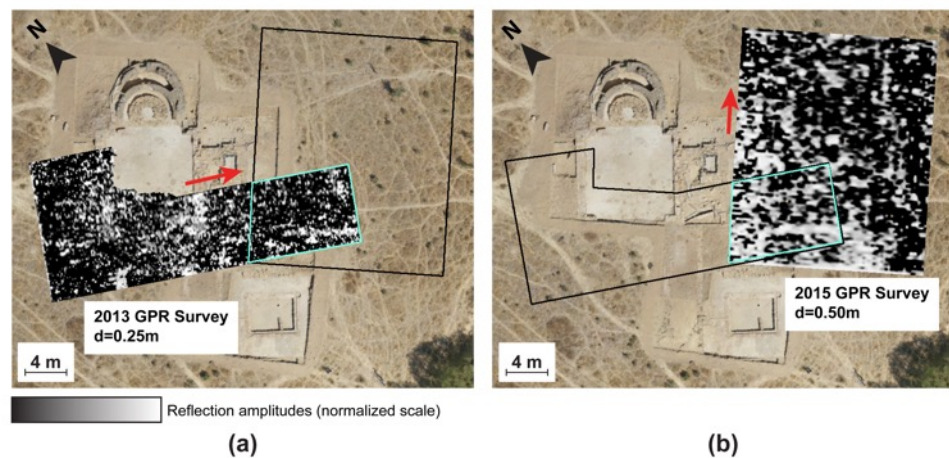


**Figure 4.** (a) Location and results of 2013 survey (profile spacing of 0.25 m). (b) Location and results of 2015 survey (profile spacing of 0.50 m). The base map is an orthophoto of Horta da Torre remains taken in 2016. The excavations took place after the GPR surveys. Arrows indicate the direction of the profiles. All the results show reflection alignments suggesting the existence of wall-type structures. The difference in profile spacing is visible in the two datasets; it mainly affects spatial resolution.

The 2013 results show reflection alignments compatible with walls and pavements (Figure 4a). The survey carried out before the archaeological excavation allows the archaeologist to guide to a place with a greater probability of the existence of a buried structure. The excavation proved that the large reflectors correspond to a wall and pavement (Figure 2a). Further excavations confirmed that this was the corridor of the east wing of the main *perystilium*.

These results highlighted an important aspect: the characteristics of this wall, its large size, robustness, and excellent condition, are not noticeable in the GPR results. The data shows that the structure exists, but they cannot report its large size.

Although the GPR results show reflectors suggesting buried structures at the site along the data processing chain, there are some issues related to data density. The data is dense with the profiles, as they have a sampling rate of 40 to 50 traces per meter, which gives a distance between traces of 0.025 m and 0.020 m, respectively. Perpendicular to the profile direction, each one is spaced 0.25 m in the 2013 survey and 0.50 m in the 2015 survey. Even if the distance between the profiles is small, there will always be a data imbalance in both directions. This question suggests that the data density can be a feature to consider. For example, it could be done with a regular square mesh during the acquisition step to avoid this transit effect of the antennas on the ground. On the other hand, the proposed approach makes it possible to increase the amount of data and information from the initial data.

## 2. Densification of 3D-GPR data with Fourier Interpolation

### 2.1. General overview of trace generation

A lateral data densification strategy is proposed based on the interpolation of GPR profiles in the spectral domain using the Fourier transform to solve the subsampling problem in 3D-GPR models. In reconstructing 2D and 3D seismic tracks, this method is widely used [5-11].

The first aspect to consider densifying a 3D-GPR dataset is that the type of information available corresponds to a spatial distribution of amplitudes,  $A(x_i, y_j, z_k)$ , resulting from the detection of reflected EMW. However, this dataset is not equally distributed in space since  $A(z_{k=1:N_k})$  represents a trace, where  $N_k$  corresponds to the number of samples, which generally has a value of 512 or 1024 samples, for spacing ( $\Delta z$ ) between 0.05 and 0.5 ns. On the other hand,  $A(x_{i=1:N_i})$  denotes the amplitude of the signal received at each point of a depth along the B-scan, where  $N_i$  denotes the number of traces in that B-scan; this defines the profile direction. Its value depends on its length and the spacing between traces ( $\Delta x$ ), usually between 1, 2, and 5 cm. Finally,  $A(y_{j=1:N_j})$  refers to the amplitudes when fixing a plane ( $x, y$ ) in which  $N_j$  corresponds to the total number of B-scans acquired during the survey, with a certain spacing between profiles ( $\Delta y$ ).

When comparing the sampling intervals considered, it becomes evident that the dataset has subsampling in the y-direction, which produces a lack of information. Therefore, an excellent strategy to increase the quality of 3D images is to densify the whole set in this direction to generate new traces between the existing parallel profiles.

For creating interpolated traces, seismic exploration processing flows offer a variety of choices. One approach utilizes mathematical transformations (such as the Fourier and Curvelet transforms) to rebuild missing features in seismic data [5, 12-14]. They map the signal in a new domain to synthesize data in spatial locations that have not been recorded [5]. Other methods rely on using the Fourier transform [15-19]. Its coefficients are calculated from the input lines to reconstruct the data for any mesh dimension [20]. In addition, there are other proposed algorithms, such as the irregular Fourier transform and sparse inversion, efficient methods in the case of regularly sampled data. All Fourier reconstruction methods require two conditions: the signal must be limited over a range of frequencies and represented by a distribution of Fourier coefficients.

The use of mathematical transforms [21] and predictive filters [22] in the  $f$ - $x$  domain [23] is one of the interpolation strategies for recovering missing traces in seismic data. We can perform the data recovery using predictive filters as autoregressive operators since linear events overlap in the  $f$ - $x$  domain. We also can apply the method to  $f$ - $x$  random noise attenuation phenomena [24-26]. For example, to interpolate data with a frequency of  $2f$ , we can use predictive filters estimated from frequency  $f$ . Predictive filters estimated from low signal frequencies, free from aliasing, are used to interpolate the content of high frequencies that suffer from aliasing and can also be used to reconstruct missing data [23, 27-28].

Automatic event identification is a technique that permits trace interpolation and allows recovery parameters or attributes [29-30]. We use the amplitudes corresponding to the reflections and arrival timings [30]. The algorithm analyzes the attributes of the recorded datasets [31–33] and converts the signal into reflection amplitudes and the cosine of the instantaneous phase. The algorithm uses the phase cosine to identify any event with lateral continuity of the phase value, connecting phases of the signal with the same polarities and close arrival times [30]. Reflection impedance allows the system to identify events in which there is a lateral variation in amplitudes or changes in the configuration of the reflected wave. The algorithm automatically connects events that have lateral coherence, defining horizons, which will then be analyzed by overlapping them with the initial profile. The analysis of each horizon intends to search for nearby subparallel events to classify them as part of the exact reflection. When grouping events, it is possible to reconstruct the reflection points by calculating the mean cosine of the phase of each horizon, preserving the reflected signal, and removing unrelated events [30].

We can apply automatic event identification to calculate spatial derivatives after applying the Fourier transform. In analogy with temporal derivatives, spatial derivatives also convert inflection points into zeros (in spatial terms), allowing any special discontinuity of seismic data to be highlighted [34]. In addition, we also can apply spectral analysis to spatial derivatives, which denotes that differentiation in the horizontal direction increases the frequency content and applies a phase shift of  $\pi/2$ . As a result, we may employ derivatives to detect small changes in the seismic signal caused by interfaces such as meshes and cracks [34].

It is also necessary to mention other data densification methods. For example, in B-scans and depth-slices, spatial interpolation may have been used. The spatial interpolation is performed by analyzing the neighboring values at the pixel level and can generate numeric artifacts without correspondence with reality. The same goes for the 3D spatial interpolation. The chosen method maintains the spectral content of the data, which provides greater effectiveness in the application of the method. Since we carry out the GPR survey by acquiring parallel profiles, the Fourier interpolation is 2D rather than 3D.

## 2.2. INT-FFT Algorithm

This study used the Fourier interpolation method to generate traces and densify the dataset in the frequency domain. The implementation is through the *Suinterp* algorithm [35], available in Seismic Unix (SU), a free access utility package from the Centre for Wave Phenomena of Colorado School of Mines (USA). This algorithm interpolates seismic traces between each pair of existing traces by applying the discrete Fourier transform to each trace and calculating the spatial derivatives of each pair of adjacent seismic traces. Then, it performs a linear interpolation between both traces in the frequency domain and applies the inverse of the Fourier transform, restoring the data to the time domain. We assume that the low-frequency content of the input signal does not suffer from aliasing and that the deeper amplitude peaks allow data interpolation across its entire bandwidth at the high frequencies that are subsampled.

The parameterization of the algorithm contains the number of lines to be interpolated between each pair of lines, the total number of traces in the profile, and corner frequency values corresponding to the GPR data frequency range.

Before applying the methodology to the entire 3D-GPR dataset, it is necessary to test with a GPR B-scan to compare the input with the output, using a profile acquired in a laboratory with a 1.6 GHz antenna. The acquisition parameters are the following: 1024 samples per trace, 5 ns temporal range, 0.004888 ns sampling interval, 196 samples per trace, 0.005 m equidistance of traces. The interpolated profile must have 391 traces, twice the traces minus one. The time range remains the same, and the distance between traces will decrease to half the initial value before interpolation, to 0.0025 m.

Figure 5a, b shows the input and interpolated B-scans. There is a slight increase in sharpness after implementing Fourier interpolation with the *Suinterp* algorithm. We also

did not notice any change in the range of amplitude values. The quality of the initial data has not decreased. We can conclude that this interpolation method works for GPR data.

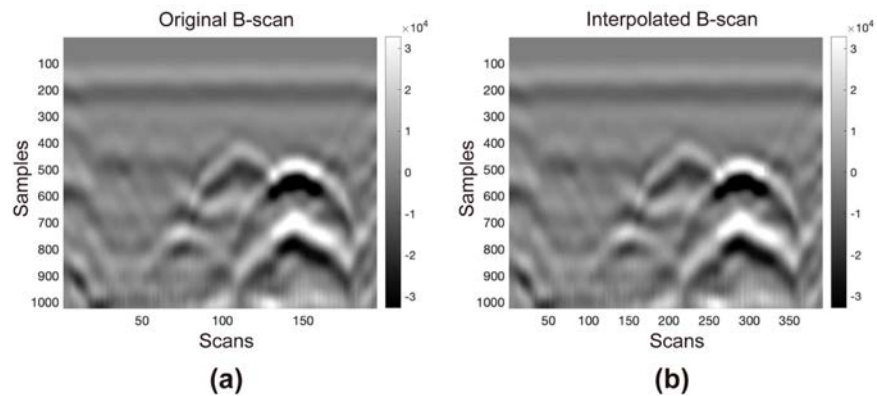


**Figure 5.** (a) Input B-scan. (b) Output B-scan after applying the Fourier interpolation through the *Suinterp* algorithm. There is no change in the initial data other than a slight increase in sharpness.

MATLAB was used to create the previous tests and the script. The *Suinterp* algorithm requires converting the GPR data to a compatible format. The adaptation of the data implies the manipulation of the matrices so that they are spatially related and so the desired information can perform the interpolation, and then the export of the matrices to the format allowed for import by the *Suinterp* algorithm.

As the data were acquired in  $N$  equally spaced parallel lines, the import of all profiles will need to store the data in the form of a 3D matrix,  $A(x_i, y_j, z_k)$ , corresponding to the spatial distribution of the lines (Figure 6a). The 3D matrix has a dimension  $(N_i, N_j, N_k)$  in which  $N_i$  and  $N_j$  are each row and column of each profile, respectively, and  $z_k$  defines the sample number of the line corresponding to the pair  $(x_i, y_i)$ .

To densify between the profiles, first, it is necessary to redefine profiles in the  $y$ -direction, meaning that the profiles to be considered will be perpendicular to the initial direction (Figure 6b). Each redefined profile consists of a trace from each original profile, sequentially ordered from  $j=1$  to  $N_j$ . This data rearrangement is necessary because the *Suinterp* algorithm interpolates a trace between each pair of traces. As a result, we need to apply the parallel profile interpolation as many times as the number of traces in the perpendicular profile. The next step is to restore the original direction of the spatial reference, redefining the profiles along the  $x$ -direction, as in the original data (Figure 6c). In total, the number of final profiles will be  $2N-1$ .

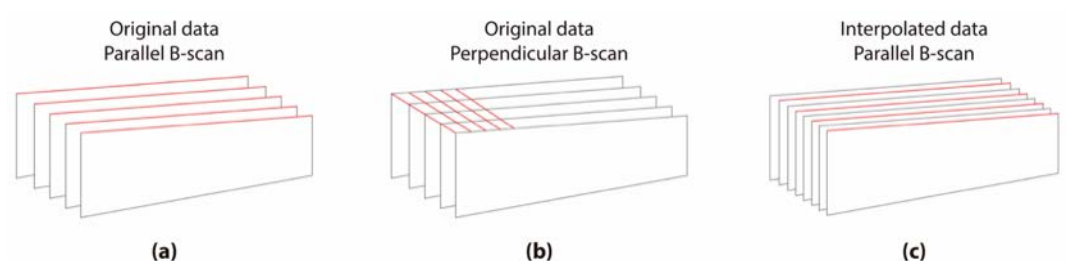


**Figure 6.** Arrangement of the 3D GPR data matrix: (a) the parallel orientation of the original profiles, inserted in the 3D data matrix; (b) perpendicular direction of the profiles, after  $90^\circ$  rotation, with the data ready to be interpolated; and (c) the parallel orientation of the profiles, after interpolation and a new  $90^\circ$  rotation, to restore the original reference frame.

The following process sequence (Figure 7) is the flow scheme to implement the densification technique in the MATLAB software:

1. Preliminary parameterization: introduction of the total number of parallel profiles and the number of the initial profile.
2. Importing GPR profiles in DZT format using routine *readgssi*, a MATLAB algorithm adapted to read files in DZT format.
3. Determination of the maximum length of the profiles so that the 3D matrix will be regular.
4. Import complementary information about the geometry of the dataset (starting and ending position of each profile); all profiles must be well located in space; during the survey, the user needs to collect all the information about the acquisition.
5. Determination of the extremes of the locations of each profile.
6. Remove the effect of the acquisition in zigzag, if necessary.
7. Normalize the length of the profiles, if necessary, by adding traces of zeros at the start or end of the profile to make the matrix regular.
8. Place the data for each profile in the 3D matrix (parallel profiles).
9. Extraction of perpendicular profiles and conversion to SEG-Y format, using the routine MATLAB *writesegy* (SegyMat Library).
10. Conversion to SU format using internal Seismic Unix routines.
11. Profile interpolation using the Seismic Unix *Suinterp* routine.
12. Importing interpolated profiles in SU format using the MATLAB *readsu* routine (SegyMat Library).
13. Place the interpolated data in the 3D matrix.
14. Extraction of parallel profiles (original + interpolated).
15. Data conversion to DZT format, using the MATLAB *writegssi* routine, developed to write files in DZT format.

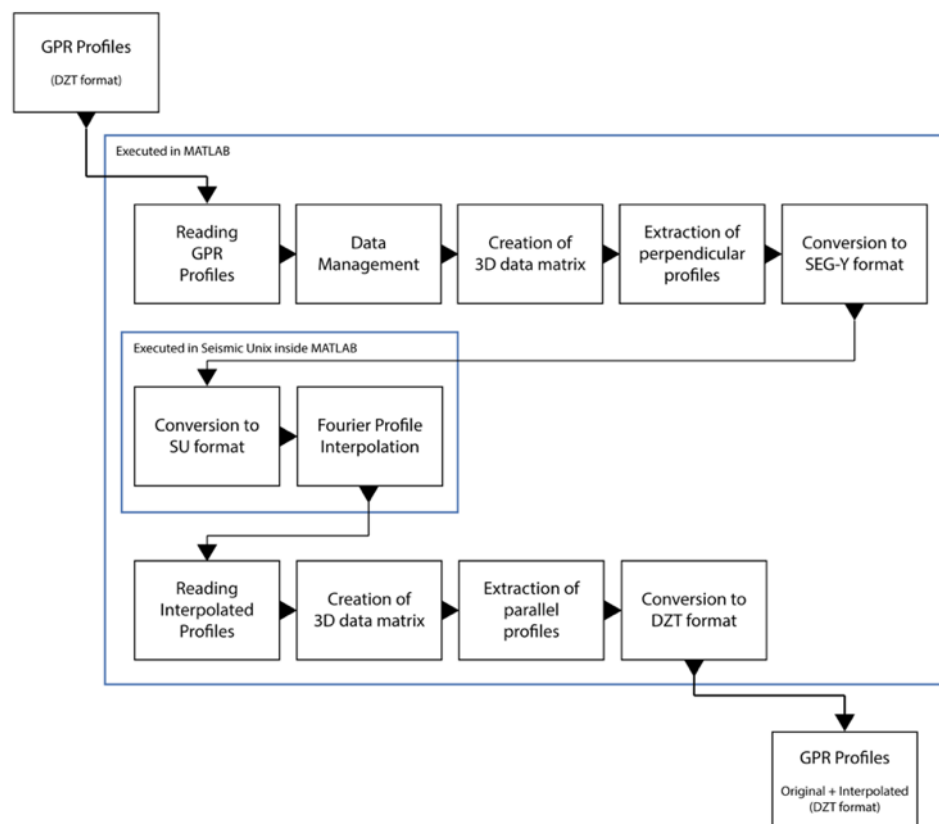


**Figure 7.** Schematics of the numerical implementation of the INT-FFT algorithm.

### 2.3. Parameters to evaluate the results

The evaluation of the results of this procedure will be by establishing comparisons between the different datasets. In addition, we will be performing an analysis of the graphical representation of the results and quantitative analysis of the Structural Similarity Index and Sharpness Index.

The Structural Similarity Index (SSI) quantifies the similarity between two datasets [36]. The result can be represented graphically (displayed differences) and in percentage (100 % corresponds to the same data).

The Sharpness Index (SI) is a parameter that quantifies the sharpness of an image with dimension ( $m \times n$ ). To calculate it, we can use the Hudgin gradient ( $dH$ ) of the image [37]; it is used in image fusion to select the sharpest pixels [38] considering the neighboring pixels. The numerical implementation requires calculating the horizontal components of the Hudgin gradient  $dxH$  and vertical  $dyH$ . These coefficients are needed to calculate the gradient modulus, used in the SI calculation [39], through Equation 1.

$$\text{Sharpness Index} = 100 * \sum_{i,j}^{m,n} \frac{\sum_{i,j}^{m,n} |dH_{i,j}|}{m \times n} \quad (1)$$

Where  $m \times n$  is the dimension of the matrix, and  $i,j$  defines the coordinates of each cell.

The increase in the Hudgin gradient values of the image occurs the more contrasted the image is. We can consider that the sharpness of an image must be associated with the diversity of contrasts: the more significant and more abundant the contrasts, the greater this index.

### 3. Results

#### 3.1. 2013 GPR dataset

The original dataset was used as input in INT-FFT algorithm to produce the interpolated dataset. We apply standard processing flow<sup>1</sup> to this dataset, with the necessary changes due to the reduced profile spacing. The approach is the same as previously described. Some tests were necessary to evaluate it.

Therefore, the pairs of datasets to consider for method analysis are the following:

- 1) Original data, C0 (d=0.250m) versus interpolated data, C1 (d=0.125m): To assess the effects of Fourier interpolation on the lateral densification of GPR profiles.
- 2) Original data, C0 (d=0.250m) versus decimated and interpolated data, C2 (d=0.250m): To assess the level of missing information retrieval through Fourier interpolation; for this, we need to decimate the original data with the elimination of profiles interspersed (between every three, we erase one in the middle), to make the spacing between profiles at d=0.500m; the interpolation will reset the original spacing between profiles (d=0.250m).
- 3) Original data, C0 (d=0.250m) versus decimated data, C3 (d=0.500m): To assess what information is lost when you choose to increase the spacing between profiles to make the survey faster, which may allow increasing the prospected area.

##### 3.1.1. Original data (d=0.250m) - default dataset - C0

The original dataset, C0, was acquired in parallel profiles, spaced at 0.250 m. The processing flow applied is the same described in section 1.2. After that, we extract depth-slices from the 3D model. The considered depths are the following: 0.28; 0.33; 0.38; 0.43; 0.48; and 0.53 m. The integration thickness of all slices is the same, 0.11 m.

The depth slices between 0.33 m and 0.53 m show alignments compatible with wall-type structures. The archaeological excavation proved the existence of the walls. However, despite the alignments being quite evident in their correspondence to buried structures, there is some difficulty in individualizing these alignments at some depths. It

<sup>1</sup> GPR standard processing flow: correction of the surface position, IIR filters, constant gain adjustment, Kirchhoff migration, predictive deconvolution, FIR filters, linear gain adjustment, Hilbert transform.

may be due to the collapse of these structures, causing additional reflections, and the profile spacing. Nevertheless, these results will be considered standard and used to compare with other datasets.

The comparison of results was carried out through direct observation and by analyzing the values of the Structural Similarity Index (Table 1). We also calculate the average Sharpness Index for each set of images, which in the original data presents the average value of 11.44% (Table 2).

### 3.1.2. Interpolated data (d=0.125m) - C1

The interpolated dataset, C1, was obtained from C0 by applying INT-FFT algorithm. The original data spaced of 0.250 m turns spaced of 0.125 m, half the initial distance.

The effectiveness of the algorithm was graphically evaluated (Figure 8) by comparing the depth-slices extracted from C1 and C0 datasets. Although there is no production of artifacts originating from the interpolation process, the reflection alignments generally seem better defined and sharper in C1 depth-slices than in C0. More minor alignments, which appeared less sharp in the initial data, show the most improvement. They became more individualized and more perceptible. The other alignments were initially quite clear, and there was an increase in their definition.

The Structural Similarity Index (Table 1) presents an average value of 82.34%. The two datasets are similar, and the interpolation does not change. The average Sharpness Index is 15.30% (Table 2). There was an increase in sharpness between the interpolated and original data (+3.86%).

### 3.1.3. Decimated and interpolated data (d=0.250m) – C2

The decimation of the original data intends to examine the extent of data recovery with this interpolation approach. First, we deleted the middle profile, resulting in a shift in the distance between profiles from d=0.250m to d=0.500m. After that, we apply the INT-FFT algorithm to make the distance between profiles again equal to the initial one (d=0.250m). Figure 9 shows the graphical comparison between C2 and C0 datasets.

As in the previous case, we do not note the production of artifacts, and the interpolation allowed recovering missing information. However, it is impossible to recover all the expected information, as highlighted by the reduced definition and sharpness of the initially observed reflection alignments. The average value of the Structural Similarity Index (Table 1) decreased to 64.15% (- 18.19%). Likewise, the average Sharpness Index decreased (-0.76%) to 10.68% (Table 2).

### 3.1.4. Decimated data (d=0.500m) - C3

Finally, we establish the comparison between the original and decimated data (Figure 10) to assess the level of information lost when the spacing between profiles increased. We compare results from C0 (d=0.250m) with those produced with decimated data from the previous case (d=0.500m), C3. The graphical analysis of decimated data allows us to verify that the definition of the reflection alignments observed in C0 has considerably decreased. However, it is still possible to distinguish the more robust alignments. The mean value of the Structural Similarity Index (Table 1) decreased to 64.74% (-17.60%).

It is essential to highlight a detail verified after the graphical analysis between decimated data, C3, and decimated and interpolated data, C2 (Figure 11). The INT-FFT algorithm can correctly reconstruct some information does not present in the decimated data. For example, the average Sharpness Index of C3 is 8.63 % (Table 2), Lower than the value observed in C0 (-2.81%).

**Table 1:** Structural Similarity Index between different datasets at different depth-slices.

Depth (m)	Structural Similarity Index (%)		
	C0 versus C1	C0 versus C2	C0 versus C3
0.28	81.17	62.49	62.78
0.33	82.50	63.02	62.62
0.38	82.44	64.98	65.49
0.43	82.65	64.16	65.23
0.48	82.66	65.10	65.47
0.53	82.62	65.17	66.87
Mean	82.34	64.15	64.74

**Table 2:** Sharpness Index between different datasets at different depth-slices.

Depth (m)	Sharpness index (%)			
	C0	C1	C2	C3
0.28	13.14	17.80	12.30	9.88
0.33	12.13	15.79	11.09	8.99
0.38	11.22	14.96	10.47	8.51
0.43	10.64	14.23	9.83	7.99
0.48	10.93	14.43	10.08	8.18
0.53	10.60	14.60	10.28	8.25
Mean	11.44	15.30	10.68	8.63

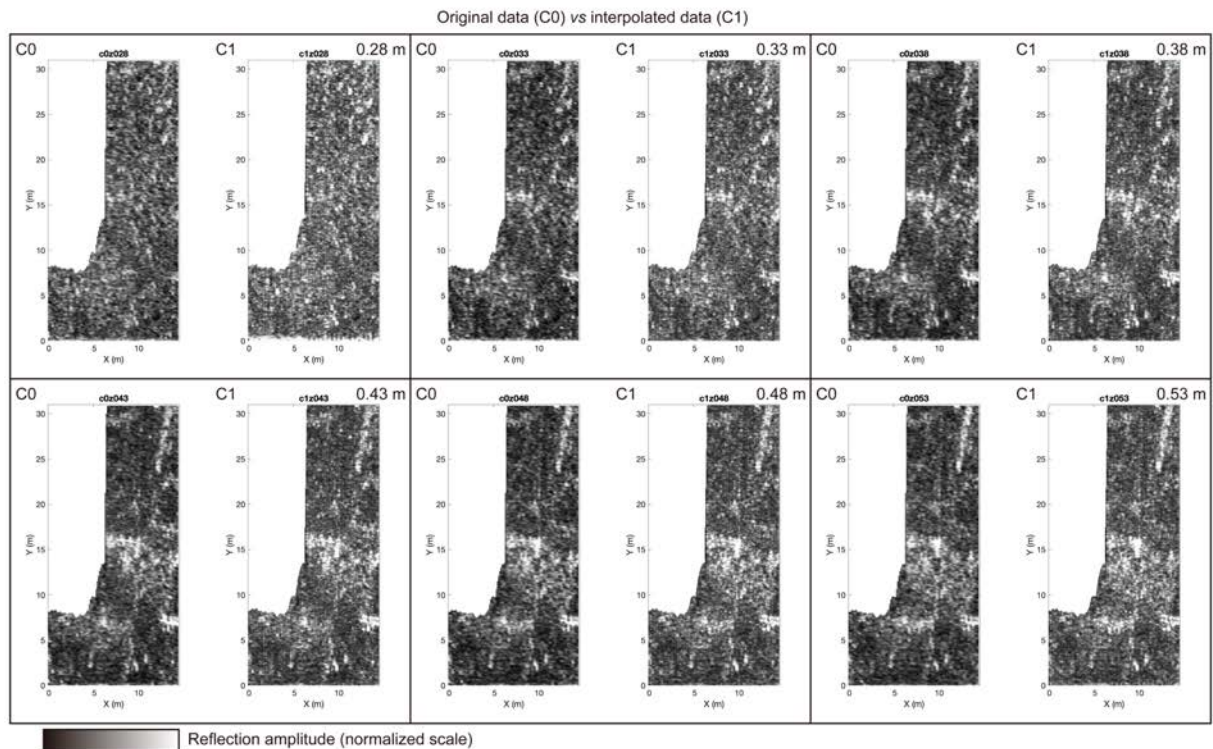


**Figure 8:** Differences between original data (C0 –  $d=0.250\text{m}$ ) and interpolated data (C1 –  $d=0.125\text{m}$ ). We can observe an increase in the definition of reflector alignments corresponding to wall-like structures after increasing the data density with the INT-FFT algorithm.

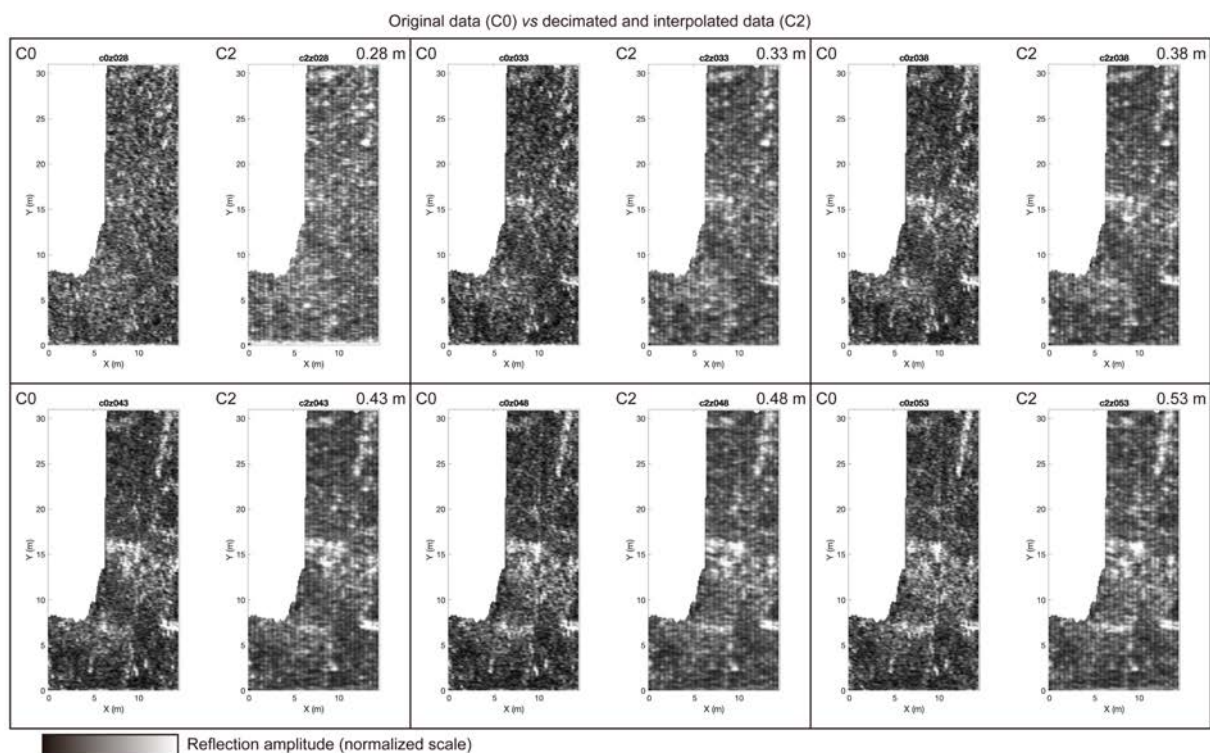


**Figure 9:** Differences between original data (C0 –  $d=0.250\text{m}$ ) and decimated and interpolated data (C2 –  $d=0.250\text{m}$ ). Data recovery after decimation and interpolation is not complete. Interpolation introduces a striped band.

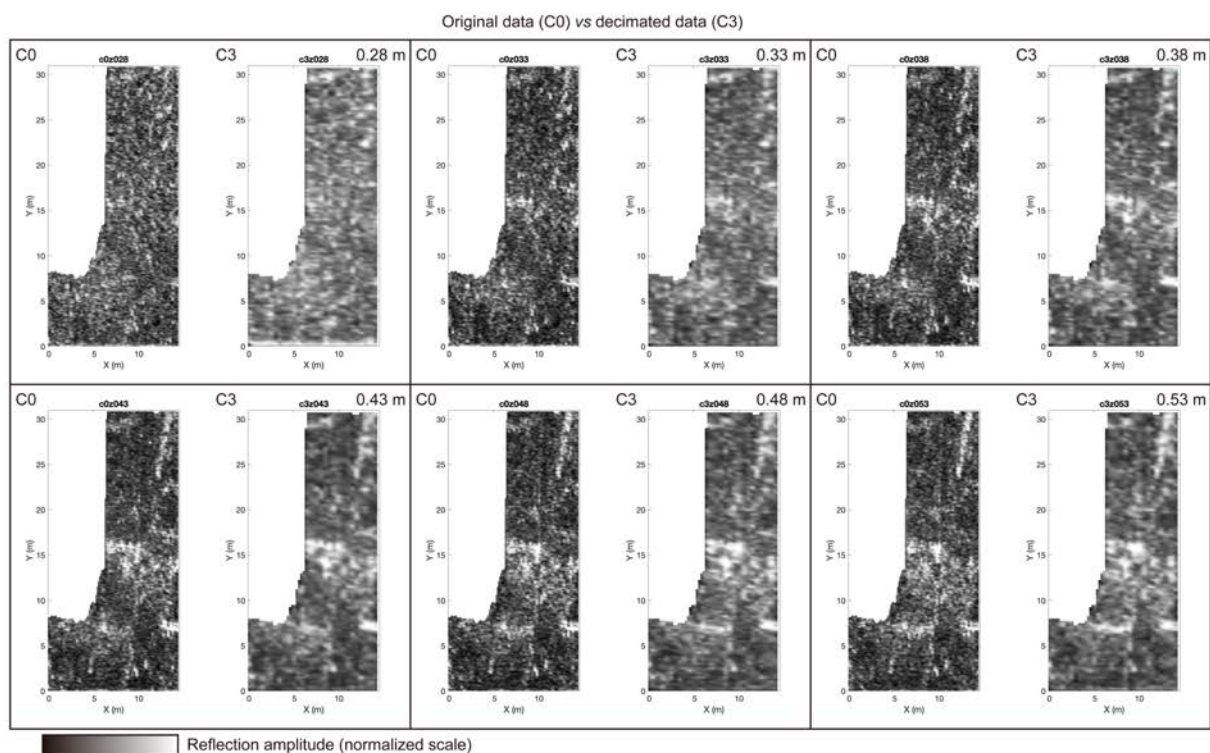


**Figure 10:** Differences between original data (C0 –  $d=0.250\text{m}$ ) and decimated data (C3 –  $d=0.500\text{m}$ ). The decimated data allow us to observe that the increase in the distance between profiles during the acquisition step impairs the evaluation.

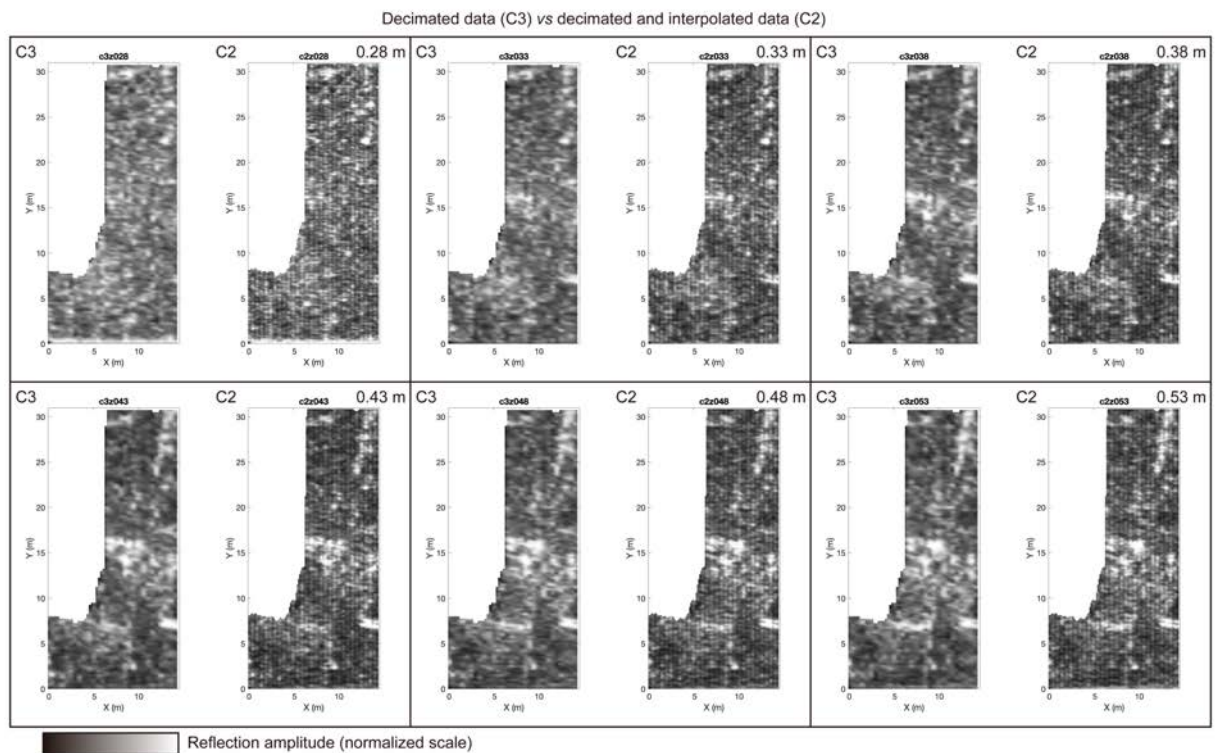
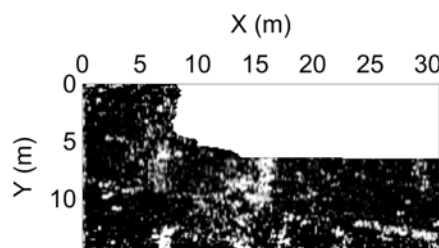


**Figure 11:** Differences between the decimated data (C3 –  $d=0.500\text{m}$ ) and decimated and interpolated data (C2 –  $d=0.250\text{m}$ ). We can assess information retrieval before and after interpolating data that we have previously decimated.

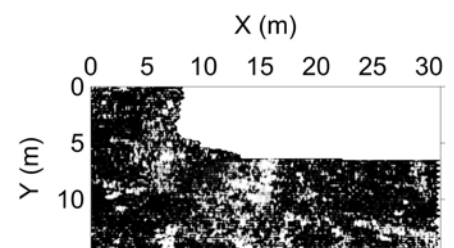
The next step is the production of cover surfaces from C0 and C1 datasets (Figure 12). This step will only consider the depth-slices between 0.38 m and 0.53 m. When we select all the depth-slices together, the cover surface will have information gaps due to slices with less information. As a result, the user must choose slices carefully. The C1 dataset shows an increase in reflection alignments corresponding to wall-type structures. There is also an increase in background reflections that appear to be noise. The Sharpness Index for both datasets increased from 13.37% to 26.19% (Table 3).

### Cover surface - Standard



(a)

### Cover surface - INT-FFT



(b)

**Figure 12:** Differences between the cover surfaces of 2013 GPR dataset: (a) standard processing; (b) after INT-FFT algorithm; and (c) after variogram correction. The data interpolation naturally amplifies the presence of background reflections that we consider noise originating from the collapse of structures and soil heterogeneities.

**Table 3:** Sharpness Index of the cover surfaces from 2013 GPR datasets, before and after INT-FFT processing. Sharpness increases with the processing applied.

GPR dataset	Sharpness Index (%)	
	Standard	INT-FFT
2013	13.37	26.19

### 3.2. GPR 2015 dataset

Another GPR dataset, gathered in 2015, was likewise subjected to the proposed technique. The distance between profiles is 0.50 m, which is higher than the 2013 dataset (0.25 m). The results obtained from a standard processing flow<sup>2</sup> in Figure 13 show reflection alignments that can correspond to buried walls. The main characteristic observed is that the alignments are not as sharp as in the 2013 dataset.

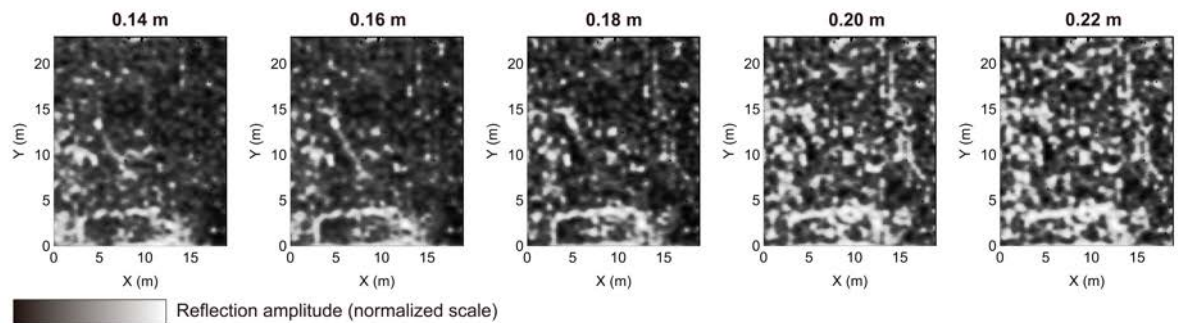


**Figure 13.** Depth-slices of 2015 GPR dataset with standard processing. The better processing of these data does not eliminate the reflections around the alignments that correspond to wall-like structures.

Applying INT-FFT algorithm to reduce the profile spacing from 0.50 m to 0.25 m, the results for each depth-slices (Figure 14) reveal that there has been an increase in data density which seems to indicate an increase in sharpness of the reflection alignments.

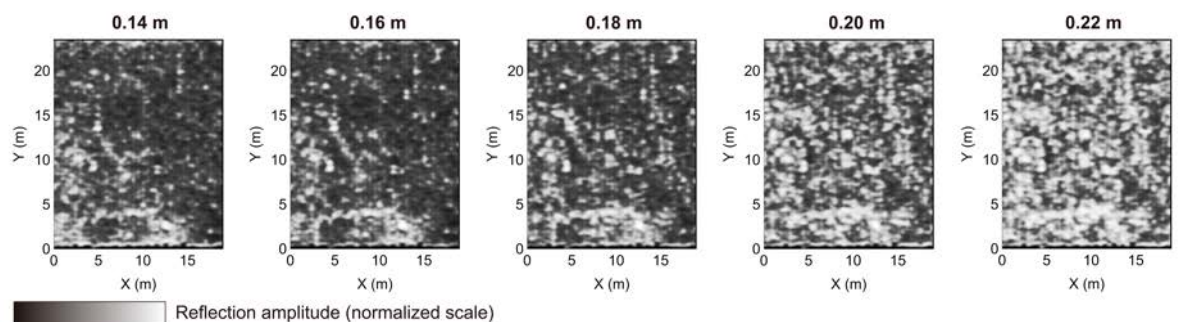


**Figure 14** Depth-slices of 2015 GPR dataset with INT-FFT processing. Data interpolation has improved the sharpness of alignments corresponding to structures. However, it also increased the reflections corresponding to background noise.

The next step is the production of cover surfaces from standard and interpolated datasets (Figure 15). Both datasets show vertical stripes in the same direction as the B-scans. The Sharpness Index for both datasets increased from 21.03% to 27.19% (Table 4).

<sup>2</sup> GPR standard processing flow: correction of the surface position, IIR filters, constant gain adjustment, Kirchhoff migration, predictive deconvolution, FIR filters, linear gain adjustment, Hilbert transform.

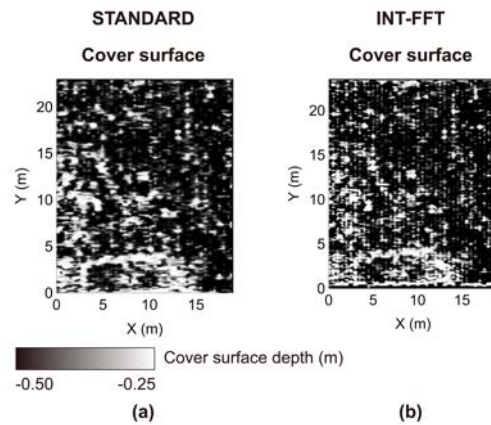


**Figure 15.** Cover surfaces obtained from several depth-slices. **(a)** Standard processing flow. **(b)** Using the INT-FFT algorithm. This type of output increases the perception of the presence of buried structures. In the interpolated data, we observe vertical strips.

**Table 4:** Sharpness Index of the cover surfaces from 2015 GPR datasets, before and after INT-FFT processing. Sharpness increases with the processing applied.

GPR dataset	Sharpness Index (%)	
	Standard	INT-FFT
2015	21.03	27.19

Due to the acquisition characteristics, such as soil grooves or dense vegetation, depth-slices and cover surfaces can present stripes with the parallel direction of the B-scans (Figure 15, top to bottom direction). We can suppress this effect by applying a directional filter to the depth-slices and cover surfaces.

There is a way to increase the coherent signal of a dataset of grid type using software such as Golden Surfer. The experimental semi-variogram can be integrated into the grid itself using geospatial statistical approaches [40]. This procedure intends to obtain information about the distribution of values located around a mesh point. The experimental semi-variogram represents the statistical trend of the spatially distributed values and can be fitted to an analytical curve and used in interpolation to generate a 2D mesh. We successfully tested this post-processing on GPR data [41], and its effectiveness is demonstrated in the 2015 GPR dataset (Figure 16).

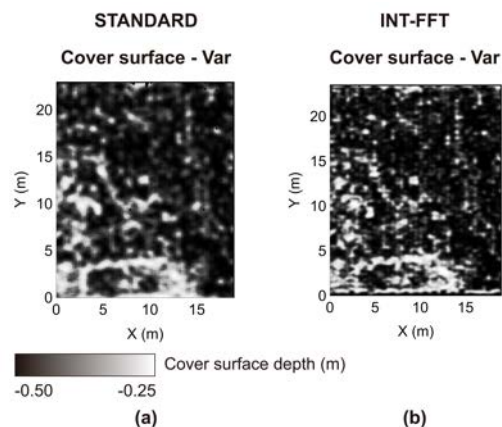


**Figure 16.** Same cover surfaces of the previous figure, obtained from several depth-slices, after removing the strip bands with a directional filter. **(a)** Standard processing flow. **(b)** Using the INT-FFT algorithm.

### 3.3. Interpretation of geophysical results in the scope of the archaeological site

After densifying the GPR datasets through the INT-FFT algorithm, it is possible to update the previous interpretation in an archaeological context by overlaying the processed cover surfaces to an aerial image obtained by an unmanned aerial vehicle (Figure 17). Yellow lines indicate structures discovered after excavation. In blue are the reflection alignments that suggest that they are wall-type buried structures.

This type of output allows us to observe that the alignments of reflections resulting from the GPR surveys correspond to structures excavated later. Likewise, the remaining alignments in unexcavated sites are consistent with the other structures. The results also show some evidence of a slight rotation in some preferred directions.

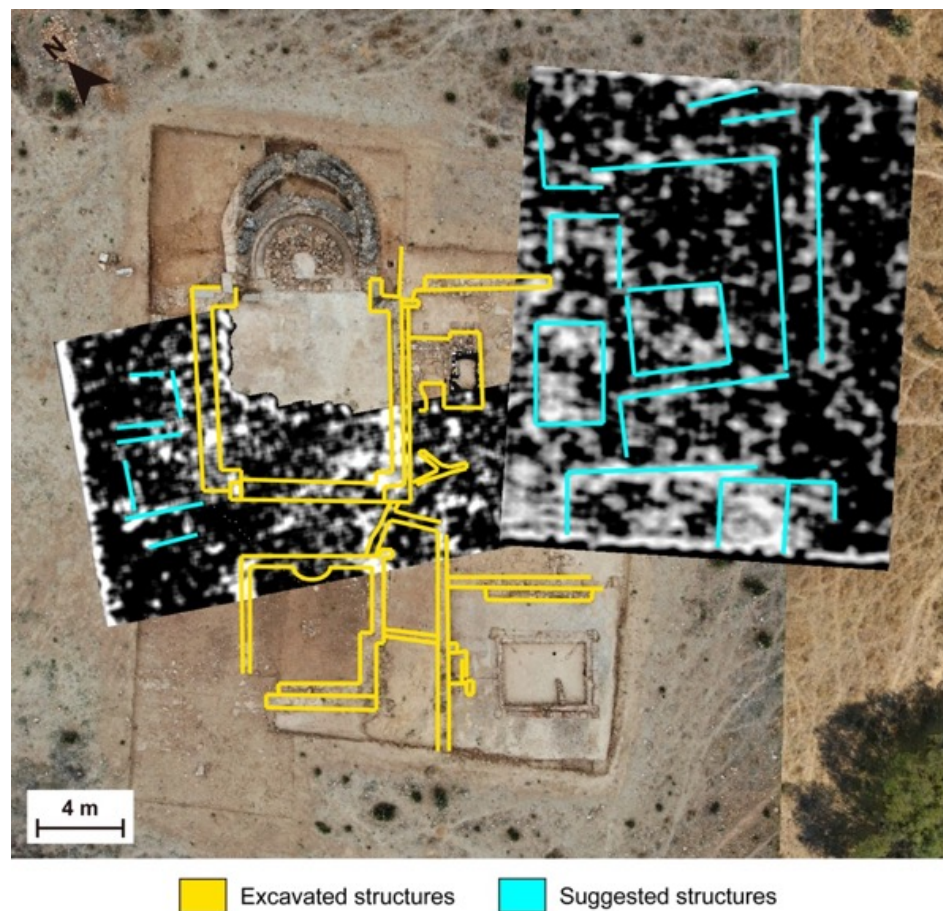


**Figure 17.** Cover surfaces from 2013 and 2015 GPR surveys after applying the INT-FFT algorithm. The outputs over an aerial orthophoto from Horta da Torre Site help interpret the results. In addition, we present a schematic representation of the visible structures (yellow lines) and the alignments obtained by the geophysical prospection (blue lines, unexcavated). INT-FFT algorithm allowed for observation reflection alignments, especially in the 2015 GPR results.

## 4. Discussion of the Results

The results obtained after implementing the INT-FFT algorithm show that the proposed approach effectively increases the lateral resolution of 3D-GPR datasets. Furthermore, data densification through 2D Fourier Interpolation allowed the creation of a new GPR B-scan between each pair of existent B-scans. Moreover, this approach increased the sharpness of the obtained GPR models.

The numerical implementation started with a test in a single B-scan to ascertain the applicability of the algorithm *Suinterp* to GPR data. The graphical aspect remains, with a change in the number of traces that increased from  $N$  to  $2N-1$ . In addition, we observed a

slight increase in the sharpness of some reflectors. The INT-FFT algorithm densifies the GPR data iteratively.

We create the algorithm based on the 2013 GPR data from Roman Villa of Horta da Torre. The survey with parallel profiles spaced 0.25 m apart has an irregularly shaped area. The short distance between profiles gives the survey a high-density character, which increases the quality of the results. We performed several tests to determine the impact of data densification using this method. The evaluation of results was performed by graphical analysis of depth-slices at several depths and by calculating parameters such as Structural Similarity Index and Sharpness Index.

The first test aimed to study the efficiency of the proposed interpolation scheme by comparing the original data (C0) and the interpolated data (C1) after applying the standard processing flow. The analysis of depth-slices at several depths shows that the alignments of reflections became more defined without the interpolation artifacts we occasionally see in the space domain. The mean value of the Structural Similarity Index of this pair of results is 82.59%. The two datasets have similar characteristics, being in tune with depth-slice analysis. Sharpness Index increased from 10.85% (C0) to 14.56% (C1).

The second test aimed to assess the missing information recovered after the data decimation, followed by interpolation by comparing the original data (C0) and the decimated and interpolated data (C2). Fourier interpolation allows us to recover the missing data. However, it does not heal it in full. Graphically, we observe a decrease in the definition of some reflector alignments. The average value of the Structural Similarity Index decreased to 64.85%. Both datasets are similar, but interpolation fails to recover the part of the missing information in the original decimated profiles without significant expression in the adjacent profiles kept. The recovery efficiency depends a lot on the object size to recover. To objects smaller than the spacing between profiles can hardly be recovered. The average Sharpness Index of the decimated and interpolated data (C2) decreased to 10.17%.

The third test evaluated the level of information lost when the spacing between profiles increases by comparing the results produced with original data (C0) and those made with decimated data (C3). The Structural Similarity Index has an average value of 65.77%, like the previous comparison. We interpret that the densification of very spaced profiles cannot reconstruct the missing data. However, the amount of information contained in the decimated dataset, compared to the original one, decreased considerably, especially the definition of the reflection alignments present in C0. Sharpness Index for an average value fell to 8.23%. However, in the C3 case, the reflection alignments allow identifying alignments of reflections compatible with wall-type structures.

The fourth test intends to compare the decimated data (C3) and the decimated and interpolated data (C2). The proposed interpolation method can reconstruct some information absent from the information contained in the existing profiles. However, it cannot reconstruct data when adjacent traces do not have lateral details. Therefore, the methodology may allow the sacrifice of the density of data acquired in the field. Nevertheless, it can be recovered in the processing step using the present interpolation technique applied in the frequency domain. However, only under conditions where the objects to be detected have dimensions that allow them to detect by adjacent profiles. In addition, the increase in profile spacing may cause under-sampling that cannot be solved.

After applying the processing flow, we need to perform a final test to the 2013 GPR dataset by calculating the cover surfaces of the C0 and C1 datasets. Graphically, C1 data became sharper than the existing reflections alignments, which the increase in the value of the Sharpness Index, which went from 13.37% to 26.19%, corroborates.

We also tested the INT-FFT algorithm on the GPR 2015 dataset obtained from the same archaeological site, with a profile spacing of 0.50 m. The results after standard processing flow show alignments of reflection that suggest buried structures of wall type, like the 2013 dataset. However, the high spacing between profiles decreases the sharpness of the reflection alignments compared to the dense dataset. After applying the

interpolation, the results show an increase in the data density, which is sharper. The improvement is more accessible to understand by analyzing the cover surfaces obtained before and after the interpolation. The increase in the values of the Sharpness Index, from 21.03% to 27.19%, also supports this improvement. In these data, we can also observe the striped effect in the direction of the profiles (vertical). Using a directional filter to correct this effect allowed its elimination, improving the data.

The combination between GPR datasets and aerial orthophoto allowed to increase the comprehension of the existence of buried structures at the site. In addition, it is possible to add interpretation schemes to highlight structures already excavated, and suggested structures only detected with GPR. Finally, it determines preferred directions that can help interpret the detected anomalies before proceeding with the excavation.

We note some limitations during method development and testing despite the approach effectiveness. Before the beginning of the interpolation process, the user needs to insert the locations of each profile. This step can be made by uploading a CSV file. However, the data input needs to be made by the user. This step implies a very well-defined knowledge of the geometry of data acquisition. Any failure of the geometric information will promote a lag of the interpolated profiles that will cause a striped effect on the interpolation outputs in the direction of the profiles. This effect may also be due to unevenness in the ground during acquisition. This graphic effect can be successfully eliminated or reduced through a correction considering the semi-variogram of the data. Another limitation is a possible slow implementation of the algorithm, even using robust hardware. The algorithm was optimized to implement the iterative interpolation process successfully. However, most of the algorithm consists of manipulating many data matrices. This process becomes slow even if the algorithm is optimized.

We also explore another aspect, determining the best processing step to implement profile interpolation. Its application was considered after completing the entire processing chain, although the results were not satisfactory. The best time to implement the INT-FFT algorithm is early in the raw data. It may be because the implemented interpolation is performed in the spectral domain, requiring that the frequency domain data have coherence by applying some processing operations, such as filtering the spectral content of the data change.

The possible advantage of Fourier interpolation applied within each profile to increase the number of traces was also explored. It was successfully used in the GPR 2015 dataset, significantly improving the data obtained.

Considering all the mentioned aspects, we can discuss the advantages of the proposed methodology over others. As implemented in the spectral domain, the INT-FFT algorithm is not a limiting factor since the computation time is constant regardless of the data. There is no production of numerical artifacts. In spatial interpolation, the speed decreases with the amount of data and the mesh size, and sometimes numerical artifacts with no correspondence to reality are created.

The continuation of this study should focus on the complete automation of the iterative process, decreasing the user dependence and optimizing the algorithm so that the computing time can reduce.

## 5. Conclusions

This study provides a new methodology for performing spectral interpolation to ground-penetrating radar (GPR) data. The densification method allows increasing the lateral resolution of 3D-GPR datasets through 2D Fourier Interpolation, creating GPR profiles between two that already existed. In addition, this approach improves the sharpness of the obtained GPR models.

The INT-FFT algorithm was tested effectively in two GPR datasets from the Roman Villa of Horta da Torre (Fronteira, Portugal). Both have distinct acquisition parameters, such as the distance between profiles (0.25 and 0.50 m) and sample rating (50 and 40

traces/m). The results show an increase in the geometric sharpness of the GPR reflectors and have not produced any numerical artifacts.

The tests performed to apply the methodology to GPR-3D data allowed us to assess the interpolation efficiency, the level of recovery of missing data, and the level of information lost when choosing to increase the distance between profiles in the acquisition stage of the data.

The use of the GPR profile interpolation methodology in the frequency domain proved advantageous in GPR-3D data densification to increase data clarity. However, we should highlight that the method only works when the data is dense enough to detect the presence of objects buried in the subsurface. Furthermore, the technique cannot generate information that is not present in the input data, so if these are under-sampled, the method will not be able to produce the missing data.

**Author Contributions:** Conceptualization, R.J.O., B.C. and T.T.; methodology, R.J.O., B.C. and T.T.; software, R.J.O. and T.T.; validation, R.J.O., B.C., T.T., J.F.B. and A.C.; formal analysis, R.J.O., B.C., T.T., J.F.B. and A.C.; investigation, R.J.O., B.C., T.T., J.F.B. and A.C.; resources, R.J.O., B.C., T.T., J.F.B. and A.C.; data curation, R.J.O., B.C., T.T., J.F.B. and A.C.; writing—original draft preparation, R.J.O.; writing—review and editing, R.J.O., B.C., T.T., J.F.B. and A.C.; visualization, R.J.O., B.C., T.T., J.F.B. and A.C.; supervision, R.J.O., B.C., T.T., J.F.B. and A.C. All authors have read and agreed to the published version of the manuscript.

**Funding:** Please add: This work has been partially supported by the research project “Innovación abierta e inteligente en la EUROACE” with the reference 0049\_INNOACE\_4\_E, by the European Union through the European Regional Development Fund included in COMPETE 2020, and through the Portuguese Foundation for Science and Technology (FCT) projects UIDB/04683/2020-ICT (Institute of Earth Sciences) and SFRH/BSAB/143063/2018.

**Conflicts of Interest:** The authors declare no conflict of interest.

## References

- Vickers, R.S.; Dolphin, L.T. A Communication on archaeological radar experiment at Chaco Canyon, New Mexico. *MASCA Newsl.* 1975, 11, 6–8.
- Conyers, L.B.; Goodman, D. *Ground-Penetrating Radar: An Introduction for Archaeologists*; AltaMira Press: Walnut Creek, CA, USA, 1997.
- Carneiro, A. Lugares, tempos e pessoas. Povoamento rural romano no Alto Alentejo. Imprensa da Universidade de Coimbra, Humanitas Supplementum nº 3, Coimbra, Portugal, 2014.
- Peña, J. A.; Teixidó, T. Cover Surfaces As a New Technique for 3D Gpr Image Enhancement. *Archaeological Applications. RNM104 - Informes. Universidad de Granada - Instituto Andaluz de Geofísica*, 2013, 1–10.
- Liu, W.; Cao, S.; Li, G.; He, Y. Reconstruction of seismic data with missing traces based on local random sampling and curvelet transform. *J. Appl. Geophys.* 2015, vol. 115, pp. 129–139.
- Gülünay, N. Seismic trace interpolation in the Fourier transform domain. *Geophysics* 2003, 68(1), 355–369.
- Liu, B.; Sacchi, M. D. Minimum weighted norm interpolation of seismic records. *Geophysics* 2004, 69(6), 1560–1568.
- Spitz, S. Seismic trace interpolation in the FX domain. *Geophysics* 1991, 56(6), 785–794.
- Naghizadeh, M. Seismic data interpolation and denoising in the frequency-wavenumber domain. *Geophysics* 2012, 77(2), V71–V80.
- Gan, S.; Wang, S.; Chen, Y.; Zhang, Y.; Jin, Z. Dealised seismic data interpolation using seislet transform with low-frequency constraint. *IEEE Geoscience and remote sensing letters* 2015, 12(10), 2150–2154.
- Wang, B.; Zhang, N.; Lu, W.; Wang, J. Deep-learning-based seismic data interpolation: A preliminary result. *Geophysics* 2019, 84(1), V11–V20.
- Bai, L. S.; Liu, Y. K.; Lu, H. Y.; Wang, Y. B.; Chang, X. Curvelet-domain joint iterative seismic data reconstruction based on compressed sensing. *Chinese Journal of Geophysics* 2014, 57(9), 2937–2945.
- Zhang, H.; Chen, X.; Li, H. 3D seismic data reconstruction based on complex-valued curvelet transform in frequency domain. *Journal of Applied Geophysics* 2015, 113, 64–73.
- Kim, B.; Jeong, S.; Byun, J. Trace interpolation for irregularly sampled seismic data using curvelet-transform-based projection onto convex sets algorithm in the frequency–wavenumber domain. *Journal of Applied Geophysics* 2015, 118, 1–14.
- Duijndam, A. J. W.; Schonewille, M. A.; Hindriks, C. O. H. Reconstruction of band-limited signals, irregularly sampled along one spatial direction. *Geophysics* 1999, vol. 64, no. 2, pp. 524–538.
- Hindriks, K.; Duijndam, A. J. W. Reconstruction of 3-D seismic signals irregularly sampled along two spatial coordinates. *Geophysics* 2000, vol. 65, no. 1, pp. 253–263.

17. Sacchi, M. D.; Ulrych, T. J. High-resolution velocity gathers and offset space reconstruction. *Geophysics* 1995, vol. 60, no. 4, pp. 1169–1177.
18. Trad, D.; Ulrych, T.; Sacchi, M. Latest views of the sparse Radon transform. *Geophysics* 2003, vol. 68, no. 1, pp. 386–399.
19. Xu, S.; Zhang, Y.; Pham, D.; Lambaré, G. Antileakage Fourier transform for seismic data regularization. *Geophysics* 2005, vol. 70, no. 4, pp. V87–V95.
20. Xu, S.; Zhang, Y.; Lambaré, G. Antileakage Fourier transform for seismic data regularization in higher dimensions. *Geophysics* 2010, vol. 75, no. 6, pp. WB113–WB120.
21. Spitz, S. Seismic trace interpolation in the F-X domain. *Geophysics* 1991, vol. 56, no. 6, pp. 785–794.
22. Andersson, F.; Morimoto, Y.; Wittsten, J. A variational formulation for interpolation of seismic traces with derivative information. *Inverse Probl.*, 2015, vol. 31, no. 5.
23. Naghizadeh, M.; Sacchi, M. D. f-x adaptive seismic-trace interpolation. *Geophysics* 2009, vol. 74, no. 1, pp. V9–V16.
24. Canales, L. L. Random noise reduction. *SEG Technical Program Expanded Abstracts 1984*, 1984, pp. 525–527.
25. Sacchi, M. D.; Kuehl, H. FX ARMA filters. *SEG Technical Program Expanded Abstracts 2000*, pp. 2092–2095.
26. Soubaras, R. Signal-preserving random noise attenuation by the f-x projection. *SEG Technical Program Expanded Abstracts 1994*, pp. 1576–1579.
27. Abma, R.; Kabir, N. Comparisons of interpolation methods. *Lead. Edge* 2005, vol. 24, no. 10, pp. 984–989.
28. Naghizadeh, M.; Sacchi, M. D. Multistep autoregressive reconstruction of seismic records. *Geophysics* 2007, vol. 72, no. 6, p. V111.
29. Chopra, S.; Marfurt, K. J. Seismic attributes - A historical perspective. *Geophysics* 2005, vol. 70, no. 5, pp. 3SO–28SO.
30. Dossi, M.; Forte, E.; Pipan, M. Application of attribute-based automated picking to GPR and seismic surveys. *NGTTS 2015, Sessione 3.3*, pp. 141–147.
31. Barnes, A. E. Theory of 2-D complex seismic trace analysis. *Geophysics* 1996, vol. 61, no. 1, pp. 264–272.
32. Barnes, A. E. A tutorial on complex seismic trace analysis. *Geophysics* 2007, vol. 72, no. 6, pp. W33–W43.
33. Taner, M. T.; Koehler, F.; Sheriff, R. E. Complex seismic trace analysis. *Geophysics* 1979, vol. 44, no. 6, pp. 1041–1063.
34. Russell, B.; Ribordy, C. New edge detection methods for seismic interpretation. *CREWES Research Report 2014*, 67, 26.
35. Andersen, J. SUINTERP revision 1.15 - interpolate traces using automatic event picking (Seismic Unix Routine – open source). Centre for Wave Phenomena - Colorado School of Mines, 2011.
36. Wang, Z.; Bovik, A. C.; Sheikh, H. R.; Simoncelli, E. P. Image Quality Assessment: From Error Visibility to Structural Similarity. *IEEE Transactions on Image Processing* 2004, 13(4).
37. Paul, S.; Sevcenco, I. S.; Agathoklis, P. Multi-exposure and multi-focus image fusion in gradient domain. *Journal of Circuits, Systems and Computers* 2016, 25(10), 2–3.
38. Yang, Y.; Huang, S.; Gao, J.; Qian, Z. Multi-focus image fusion using an effective discrete wavelet transform based algorithm. *Measurement Science Review* 2014, 14(2), 102–108.
39. Birdal, T. (2022). Sharpness Estimation From Image Gradients. *MATLAB Central File Exchange*. Available online: <https://www.mathworks.com/matlabcentral/fileexchange/32397-sharpness-estimation-from-image-gradients> (accessed on 13 April 2022).
40. Matheron, G.; Armstrong, M. *Geostatistical case studies*; Springer Science & Business Media, 2012.
41. Oliveira, R. J. *Prospecção Geofísica aplicada à Arqueologia*. PhD Thesis in Earth and Space Sciences (Geophysics), Institute of Research and Advanced Training, University of Évora, Évora, Portugal, 2020.